RSC Advances

PAPER

View Article Online
View Journal | View Issue

Cite this: *RSC Adv.*, 2026, **16**, 6069

N-doped carbon quantum dots for the detection of 4-nitrophenol, antioxidant activity, and synthesis of Fe_3O_4CuO@CQD as a catalyst for the reduction of 4-nitroaniline

Namrata Priyadarshini Hota, Prakash Seenu, Nandhini Karthikeyan, Naveen Murugan and Sathiyanarayanan Kulathu Iyer *

Received 3rd January 2026
Accepted 8th January 2026

DOI: 10.1039/d6ra00058d

rsc.li/rsc-advances

In this work, raw turmeric and L-arginine were used as the source in the hydrothermal process to synthesize nitrogen-doped carbon quantum dots (NCQDs) in an environmentally friendly, greener manner. Because of their excellent photoluminescence, quantum yield of 36.40%, and their water solubility, the NCQDs were investigated for their multifunctional applications. As a result, they were used as a sensor for the selective detection of 4-nitrophenol (4-NP). 30 nM was determined to be the limit of detection (LoD). It also shows strong antioxidant efficacy, which was evaluated using DPPH free radical scavenging. Additionally, the NCQDs stabilized the synthesis of the FeO_4CuO@CQD nanocomposite and were characterized using various methods to ascertain their catalytic efficiency. Subsequently, 4-nitroaniline (4-NA) was reduced to *p*-phenylenediamine aided by these nanocomposites.

1 Introduction

In the rapidly evolving field of nanotechnology, carbon quantum dots have garnered significant recognition for their exceptional optoelectronic and chemical properties.[1] Being a carbon material of the new generation, carbon dots typically exhibit unique photoluminescence behavior, excellent water solubility, and biocompatibility, and are environmentally friendly, with sizes less than 10 nm.[2,3] All these characteristics distinguish carbon dots from other traditional semiconductors, especially those containing toxic metals.[4,5] The versatility of carbon dots' properties, achieved through surface specification, nitrogen, and phosphorus doping, enables their use in a wide range of applications, including sensing, bioimaging, antibacterial, antimicrobial, antioxidant activities, and catalysis.[6–11]

The synthetic strategies of the carbon dots could be broadly distinguished into two categories: top-down and bottom-up strategies.[12] The top-down approaches involve breaking down larger molecules of carbon materials into nanoscale by the use of different chemical and physical technologies like arc discharge,[13] laser ablation,[14] electrochemical oxidation,[15] and acid-mediated exfoliation.[16] It is costly, synthesised using harsh conditions, and generally the quantum yield is very less. On the other hand, the bottom-up strategies involves the synthesis of CQD from small organic molecules and are natural and from eco-friendly precursors. The bottom-up approaches are constructed through chemical or thermal technologies, such as hydrothermal,[17] solvothermal,[18] pyrolysis,[19] and microwave radiation.[20]

Green and sustainable synthesis approaches have led to further evolution of nanomaterials in recent years. With that goal, the development of carbon dots using a sustainable approach is emerging due to their low cost and biodegradable nature.[21] In this context, turmeric could be an option for the sustainable synthesis of carbon dots. Turmeric is widely known for its medicinal uses, including anti-inflammatory, antioxidant, anticancer, and antimicrobial activities.[22] It is an abundant source of polyphenols and diketone groups, making it a better choice for the synthesis of carbon dots. On the other hand, L-arginine is a semi-essential amino acid and it contains an amino and carboxylic acid groups, which could be a greater choice as a nitrogen doping that can be attributed to the sustainable and eco-friendly strategies.[23]

The incorporation of L-arginine with turmeric for the synthesis of carbon dots yields N-doped CQDs that enhance the optical and functional properties. The surface of the carbon dots contains various functional groups, such as –OH, –COOH, and $–NH_2$,[24] which allows them to incorporate various applications, such as environmental sensing, which includes the detection of toxic pollutants, metals, and analytes.[25] In addition to sensing, these CQDs could play a crucial role in antioxidant activities as it is derived from turmeric, which is a better choice for it. The surface group of the carbon dots donates its electrons or hydrogen atoms to neutralize the reactive oxygen species, such as hydroxyl and superoxide radicals.[26] Even while research

Department of Chemistry, School of Advanced Sciences, Vellore Institute of Technology, Vellore-632 014, India. E-mail: sathiyanarayanank@vit.ac.in

on CQDs is advancing quickly, there are still many unresolved issues. Many reported CQDs' limited multifunctionality, usage of hazardous precursors, and complicated synthetic processes prevent them from being used in real-time applications. Additionally, a few integrated systems exist that merge real-time applications such as metal nanoparticle inclusion, therapeutic activities, and sensing into a single environmentally friendly platform. Thus, developing a sustainable, multipurpose CQDs pathway for both real-time applications and environmental monitoring at the same time is extremely desirable.

Apart from sensing and antioxidant activity, CQDs are used as a scaffold or stabilizer, and a reducer for the synthesis of metal and metal oxide nanoparticles.[27] These metal or metal oxide nanoparticles act as catalysts, catalyzing the reduction of various organic compounds and the reduction of organic pollutants'.[28] Nitroarenes are among the most hazardous chemicals derived from industrial waste, dyes, and pesticides, and are highly soluble in water. Eliminating these toxic materials is very crucial for the environment as well as the aquatic life.[29,30]

In order to demonstrate a green nanotechnological approach, we have created carbon quantum dots in this study utilizing turmeric and L-arginine as a sustainable and natural source. Because of their special fluorescent and therapeutic qualities, NCQDs can be employed as a fluorescent sensor for 4-nitrophenol (4-NP) sensing and for DPPH radical scavenging. Besides, these NCQDs stabilize the synthesis of the Fe_3O_4-CuO@CQD nanocomposite. Additionally, this nanocomposite reduces 4-nitroaniline by acting as a catalyst.

2 Experimental

2.1 Materials

All chemicals and solvents used in the analytical studies were purchased from reputable suppliers, including Avra Chemicals, Sigma-Aldrich, and TCI Chemicals. Using a JASCO 4100 spectrometer, Fourier-transform infrared (FTIR) spectra were captured. A Hitachi UV-vis spectrophotometer (Model U-2910) was used to detect UV-visible absorption spectra. Utilizing a Hitachi F-7000 fluorescence spectrophotometer, emission studies were carried out. FeO_4 nanoparticles were analyzed by powder X-ray diffraction (PXRD) using a Bruker D8 Advance diffractometer.

2.2 Preparation of NCQD

Turmeric extract was selected as a more environmentally friendly source for the one-step hydrothermal process of producing the NCQD, and L-arginine was used to dope the nitrogen. Fresh turmeric was first dried, debris-freed, and left to sun-dry for three days before being milled into a fine powder. 1 gram of the powder and 250 mg of L-arginine were combined with 50 mL of distilled water and placed in a Teflon autoclave, which was then heated at 180 °C for 6 h. A turmeric-to-L-arginine ratio of 1 : 0.25 was chosen to add enough nitrogen without going overboard, which could have a detrimental effect on fluorescence due to non-radiative recombination. The reaction mixture was allowed to reach room temperature once the reaction was finished, and then it was filtered and centrifuged for 15 minutes at 10 000 rpm. After that, the synthesized NCQD was stored in a refrigerator for subsequent procedures, as shown in Fig. 1.

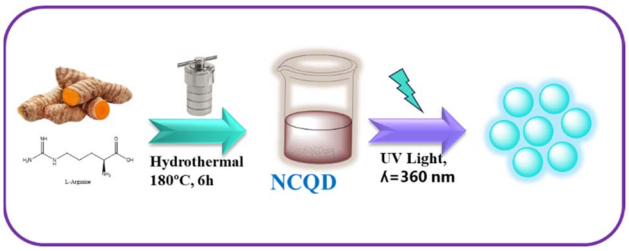

Fig. 1 Synthesis of the NCQD.

2.3 Fluorescent detection of 4-NP

For the fluorescence detection of 4-NP, 2 mL of the NCQD (diluted 50 times from the stock solution) was placed in a quartz cuvette. The cuvette containing NCQD was filled with 100 μL of 4-NP (1 mmol) and thoroughly mixed. A spectrophotometer was used to record the fluorescence spectra, with the excitation wavelength maintained at 360 nm. Following the addition of 4-NP to the NCQD, a progressive decrease in fluorescence intensity was noted. However, the spectra showed a negligible change when other analytes were added to the NCQD, confirming that it is only detecting 4-NP.

2.4 Protocols for antioxidant activities

The radical scavenging activity or the antioxidant activity of the NCQD was analyzed using the DPPH (2,2-diphenyl-1-picrylhydrazyl) radical scavenging method, which is reported by Shimada *et al.* (1992).[31] Concisely, 4 mL of the NCQD of different concentrations were mixed with 1.0 mL of 0.2 mM DPPH solution, which was prepared using 80% of methanol. The reaction mixture was vigorously shaken and incubated in a dark room for half an hour. After that, the absorbance was measured at 517 nm using UV-vis analysis, and butylated hydroxytoluene (BHA) was the positive control for it. The % of DPPH radical scavenging was calculated using the formula;

$$\%\ \text{of inhibition}(I) = \frac{A_0 - A_1}{A_0} \times 100$$

where A_0 is the absorbance of the control, and A_1 is the absorbance of the NCQD.

2.5 Synthesis of Fe_3O_4/CuO@CQD nanocomposite

The Fe_3O_4/CuO@CQD nanocomposite was synthesized by dispersing 50 mg of previously made Fe_3O_4 nanoparticles and CuO nanoparticles (S2 and S3) in 50 mL of water in a sonicator for approximately 15 minutes. Then, while stirring constantly, 20 mL of the NCQD was added to the dispersed solution. Then, for two hours, the reaction mixture was stirred at 80 °C to guarantee that the NCQD was uniformly stabilized on both

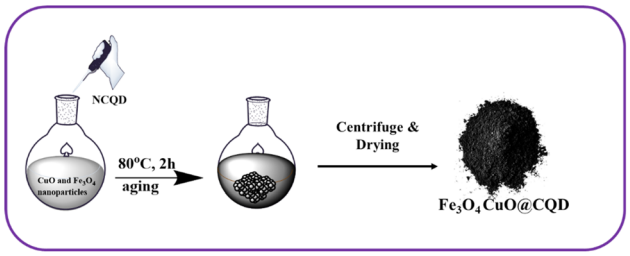

Fig. 2 Synthesis of the Fe_3O_4/CuO@CQD.

metal oxide surfaces. Two hours later, the black precipitate of the Fe_3O_4/CuO@CQD nanocomposite was allowed to reach room temperature before being centrifuged to get rid of the impurities that were soluble in ethanol and water. The nanocomposite was allowed to dry in an oven following centrifugation as in Fig. 2.

2.6 Catalytic reduction of 4-nitroaniline

Specifically, 10 mL of an aqueous solution of 4-nitroaniline (0.025 mM) and 10 mL of an aqueous solution of $NaBH_4$ (0.025 M) were placed in a beaker, and 2 mg of the Fe_3O_4/CuO@CQD catalyst was added. After that, at room temperature, the entire solution mixture was agitated. At regular intervals, UV-visible spectra were used to monitor the progress of the reaction. After a while, the solution's color changed from dark yellow to pale yellow, indicating that 4-nitroaniline had been reduced to *p*-phenylenediamine. An excess amount of $NaBH_4$ was used to maintain pseudo-first-order reaction kinetics, allowing reliable evaluation of the catalytic efficiency.

3 Results and discussion

3.1 Characterization and optical behavior of NCQD

The FTIR analysis was conducted on the NCQD's surface, which is covered with a diverse array of functional groups. The results showed that the spectrum contained significant peaks for several of these functional groups. Fig. 3 shows that the asymmetric stretching of the –OH/NH bond is evident in the strong band at 3344 cm^{-1}.[32] The asymmetric and symmetric stretching of the aliphatic –C–H groups are associated with the peaks at 2978 cm^{-1} and 2897 cm^{-1}. A distinct peak around 1650 cm^{-1} is due to the stretching of C=O groups, demonstrating the presence of carboxylic acid, ketones, and amide groups. Similarly, the peak at 1388 cm^{-1} associated with the bending vibration of C–H, the peaks at 1083 and 1041 cm^{-1} are attributed to stretching vibration of –C–O, indicating the presence of alcohols or ether groups, and one more peak around 880 cm^{-1} is due to aromatic and unsaturated alkene groups.

The HRTEM pictures (Fig. 3b) demonstrate the development of CQDs with a quasi-spherical shape and a particle size of roughly 5–10 nm. Strong interparticle interactions lead to agglomeration, which produces both microscopic and bigger particles that range in size from 12 to 15 nm. The diffuse concentric rings in the SAED pattern demonstrate the

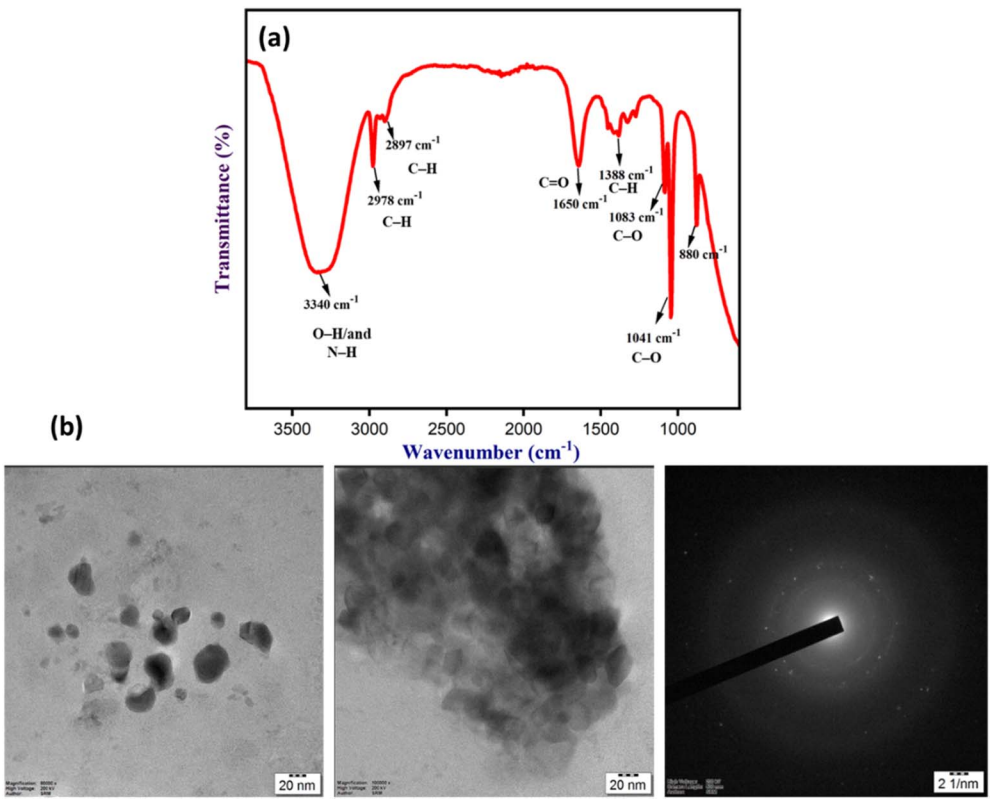

Fig. 3 (a) FT-IR analysis of NCQDs, (b) HRTEM analysis of NCQDs.

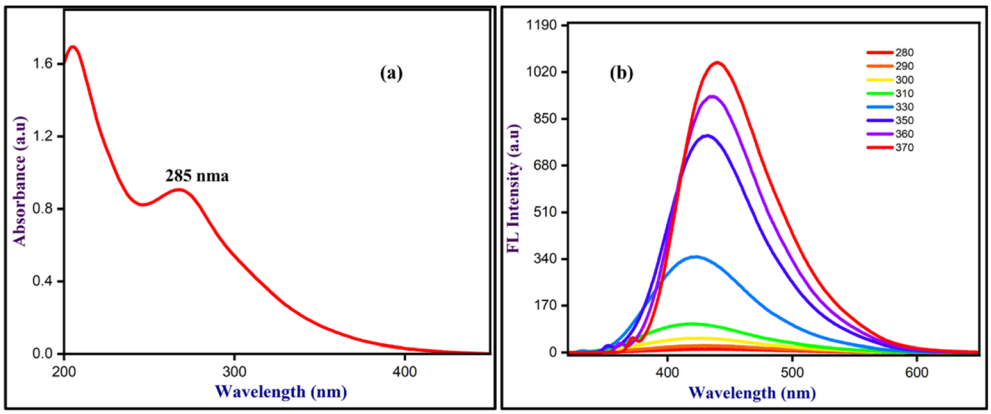

Fig. 4 (a) UV-visible analysis of NCQD, and (b) FL spectra of NCQD at different wavelengths.

amorphous carbon framework with short-range structure that characterizes carbon quantum dots.

Additionally, optical characteristics were investigated by recording UV-visible spectrum and fluorescence spectrum (Fig. 4a). The NCQD appeared yellow to the naked eye, even though they exhibited a vivid blue colour under UV light. The π–π* transition, which is induced by C=C and C=N bonds, is represented by a peak at 226 nm in the matching UV spectrum. The n–π* transition, which is induced by C=O bonds, is represented by the other peak at 285 nm. The NCQD's luminous nature was demonstrated by its vivid blue emission at 450 nm with excitation at 360 nm. Furthermore, these carbon dots exhibited excitation-dependent photoluminescence (PL), which may have been the result of defects in the size and surface of the NCQDs (Fig. 4b). Using quinine sulfate as a reference, the quantum yield of the NCQD was determined to be 36.40%. After one hour of irradiation at 360 nm, no discernible alteration in the fluorescence spectrum was observed.

Subsequently, pH investigations were conducted, wherein solutions with a pH range of 2 to 12 were prepared using 0.1 M HCl and NaOH, and a pH meter was employed to ascertain the requisite pH value. The research demonstrated that the FL intensity commenced to decrease at pH 2 and subsequently increased until it reached the neutral pH of 7. This pattern was the consequence of protonation, which was induced by functional groups such as (–OH, –NH) on the NCQD surface. The intensity was observed to decrease significantly as the pH became basic, as shown in Fig. S1.

3.1.1 Selectivity studies. The NCQD that was previously synthesized was employed as a fluorophore that was highly selective for the detection of 4-NP. A variety of competitive ions and acids, including dichloronitrobenzene (DCNB), difluoronitrobenzene (DFNB), dinitrobenzene (DNB), dinitrophenol (DNP), nitrobenzene (NB), *p*-nitroaniline (PNA), PNB (*p*-nitrobenzaldehyde), Fe^{3+}, Fe^{2+}, Ca^{2+}, Mg^{2+}, Zn^{2+}, CN^{-}, NO_3^{-} and *p*-nitrobenzoic acid (PNBA), were employed to evaluate the interaction with NCQD. The experiment consisted of two mL of 50 times diluted NCQD, and every analyte solution was added once to the NCQD. The fluorescence emission spectra were captured at 450 nm after excitation at 360 nm. The addition of 4-NP resulted in a decrease in the intensity of NCQD. The spectra demonstrated that NCQD was highly selective for 4-NP, as no other analyte altered the results (Fig. 5a). The interference studies were also observed, utilizing 2-NP, 3-NP, DCNB, DFNB, DNB, DNP, NB, PNA, PNB, Fe^{3+}, Fe^{2+}, Ca^{2+}, Mg^{2+}, Zn^{2+}, CN^{-}, NO_3^{-} and PNBA in conjunction with 4-NP to estimate the clash

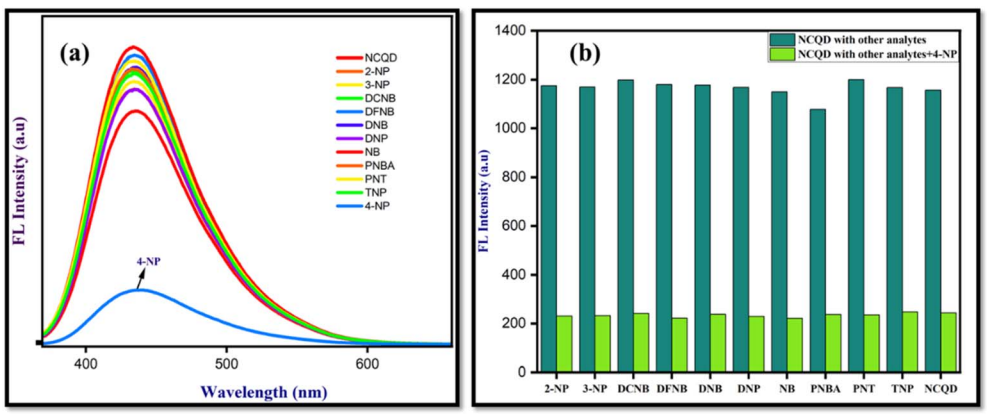

Fig. 5 (a) Selectivity study, and (b) interference study of NCQD.

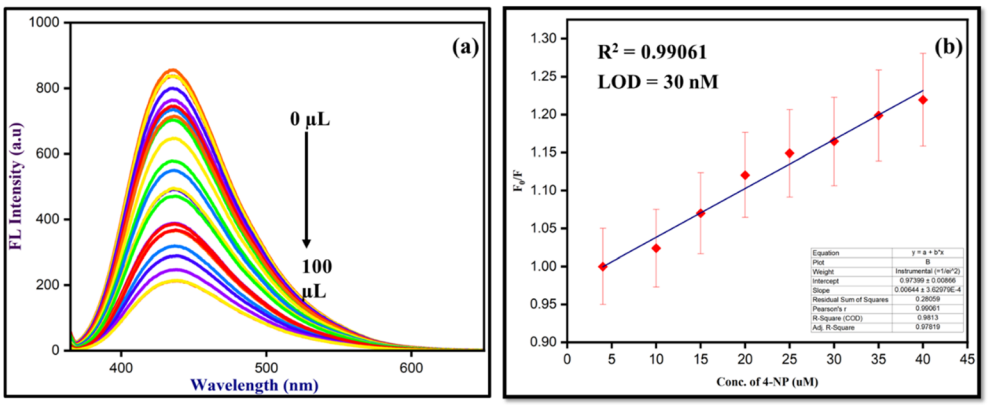

Fig. 6 (a) Titration of NCQD with 4-NP, (b) calibration plot of NCQD with 4-NP with a concentration range from 0 to 45 µm.

of other analytes on the 4-NP complex with the NCQD. The spectrum obtained was unaffected by the presence of various analytes, indicating that interference from other analytes was not present (Fig. 5b).

With increasing 4-NP concentration, the fluorescence intensity of the NCQD progressively decreased. The titration was carried out by adding up to 100 µL of 4-NP stock solution to a fixed volume of NCQD, and a rapid quenching response was observed within 5 s of 4-NP addition (Fig. 6a). Fig. 6a illustrates the fluorescence quenching behaviour as a function of added volume, while Fig. 6b shows the corresponding calibration plot constructed using the calculated 4-NP concentrations. A linear response was obtained up to 45 µM, beyond which deviation from linearity occurred due to saturation and inner filter effects; therefore, the limit of detection was evaluated within this linear range.

To evaluate the limit of detection for the NCQD, a graph depicting the relative fluorescence response of NCQD (F_0/F) against the concentration of 4-NP (in µM) was utilized, as illustrated in Fig. 6b. F_0 and F denote the fluorescence intensity before and after the introduction of 4-NP, respectively. The elevated correlation coefficient ($R^2 = 0.99627$) demonstrated a robust linear relationship within the concentration range of 0 to 40 µM. The limit of detection (LoD) was determined to be 30 nM using the specified formula.

$$\text{LOD} = 3\sigma/\text{slope}$$

The symbol σ denotes the standard deviation, and the limit of detection (LOD) for this NCQD is commensurate with that of other carbon quantum dots. A comparative table for different carbon quantum dots is located in Table S1.

3.1.2 Radical scavenging activity of NCQD. The NCQDs' antioxidant efficacy was assessed using the DPPH free radical scavenging assay, with butylated hydroxytoluene (BHT) serving as a reference. Using varying concentrations of NCQD (50–250 µL mL^{-1}), the antioxidant experiment was performed, and Fig. 7 illustrates the proportion of DPPH inhibition. It is evident that

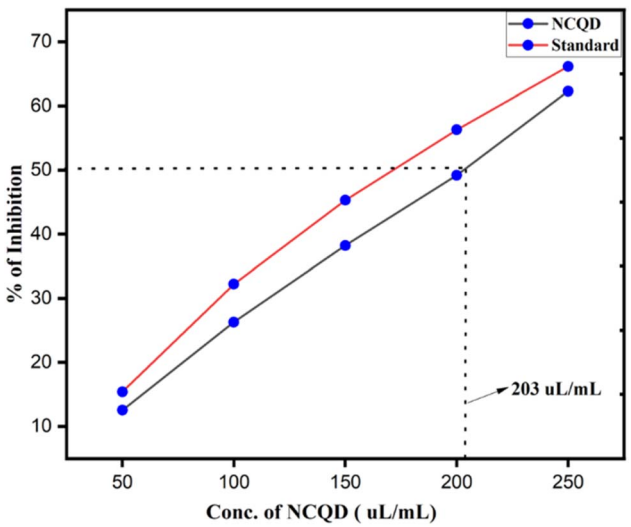

Fig. 7 Antioxidant activities of NCQD.

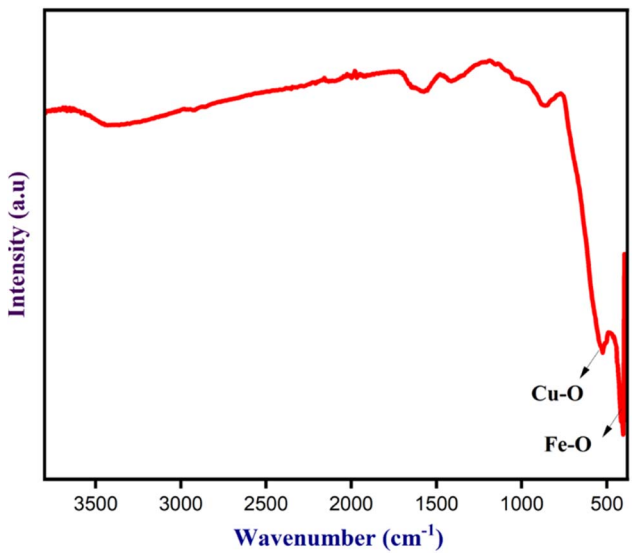

Fig. 8 FT-IR analysis of Fe_3O_4/CuO@CQD nanocomposite.

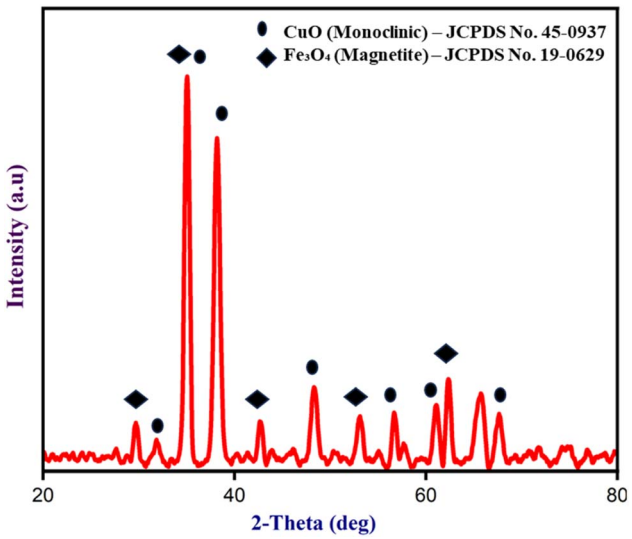

Fig. 9 *p*-XRD analysis of Fe_3O_4/CuO@CQD nanocomposite.

both BHT and NCQD have concentration-dependent radical scavenging capabilities against DPPH. The radical scavenging test showed about 63% inhibition at a concentration of 250 μL mL^{-1}, which is in good agreement with the standard BHT of 67%. Up to 13% reduction of antioxidant potential was shown even at a lower dosage of the NCQD (50 μL mL^{-1}). This demonstrates how well the NCQD neutralizes free radicals by donating electrons and hydrogen. The NCQD exhibits effective potential for the free radical scavenging activities, as evidenced by the IC_{50} value of 203 μL mL^{-1}.

3.2 Characterization and application of Fe_3O_4/CuO@CQD nanocomposite

The synthesized nanocomposite was subjected to FT-IR analysis to ascertain the bonding interactions and functional groups present in the nanocomposite. The spectra display the presence of two distinct peaks in the fingerprint region, indicating the presence of a metal–oxygen bond. The peaks around 540 and 470 cm^{-1} are assigned to Cu–O and Fe–O bonds, respectively, as shown in Fig. 8. The successful production of the composite is confirmed by the retention of broad –OH/–COOH/–NH bands, which show that the functional groups on the CQD surface are still there and help to anchor the metal oxide nanoparticles.

The Fe_3O_4/CuO@CQD nanocomposite was evaluated for phase purity, crystallinity, and structural evidence using *p*-XRD analysis (Fig. 9). It was observed that the diffractive peaks correspond to the monoclinic phase of CuO and the magnetic phase of Fe_3O_4 nanoparticles. The diffraction planes (110), (111), (200), (202), (020), (202), (113), (220), and (221) are aligned with the diffraction peaks of monoclinic CuO nanoparticles at 35.5°, 38.7°, 48.7°, 53.5°, 58.3°, 61.5°, 66.2°, and 68.0° respectively (JCPDS no. 45-0937). Similarly, the diffraction peaks at 30.1°, 35.4°, 36.9°, 43.1°, 53.4°, 57.0°, and 62.6° are attributed to the diffraction planes (220), (311), (222), (400), (422), (511), and (440) respectively, (JCPDS no. 19-0629) which confirms the presence of Fe_3O_4 nanoparticles. The average particle size of the nanocomposite was determined to be 15 nm by using the formula $D = (0.94\lambda)/\beta \cos\theta$.

FESEM analysis was employed to ascertain the surface morphology of the Fe_3O_4/CuO@CQD nanocomposite. The agglomerated spherical morphology of flake-like structure of the nanoparticles, was demonstrated by the FESEM study, as illustrated in Fig. 10.

The HRTEM image of Fe_3O_4/CuO@CQD nanocomposite shows a flake-like carbonaceous matrix formed from CQDs (Fig. 11). A heterostructured composite rather than a single crystalline phase is shown by the textured contrast. The Selected Area Diffraction (SAED) pattern shows concentric diffraction rings, indicating that the material is polycrystalline and consistent with Fe_3O_4 and CuO phases. The existence of C, O, Fe, and Cu is further confirmed by EDS analysis, confirming that the Fe_3O_4/CuO@CQD nanocomposite was successfully formed.

Thermogravimetric analysis (TGA) was done to verify the thermal stability of nanoparticles. The experiment was conducted in a nitrogen environment at a heating rate of 20 °C per minute, with a temperature range of 35 to 800 °C (Fig. 12a). The catalyst's initial 5–6% breakdown was the result of moisture absorption during the synthesis phase. Due to the reduction of

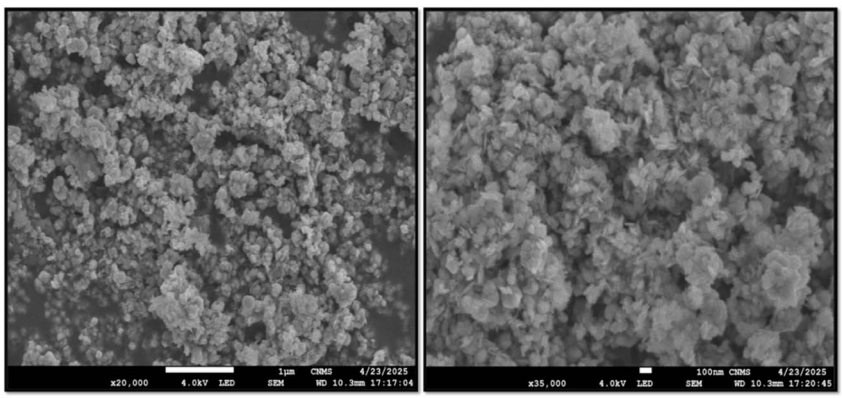

Fig. 10 FESEM analysis of Fe_3O_4/CuO@CQD nanocomposite.

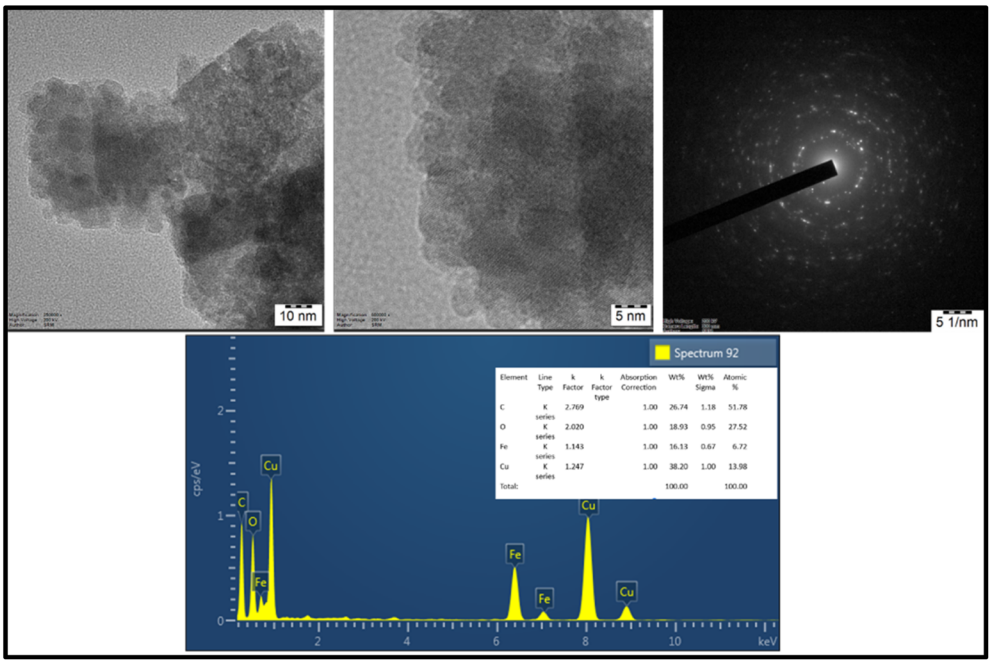

Fig. 11 HRTEM analysis of Fe_3O_4/CuO@CQD nanocomposite.

volatile solvents in the NCQD, a substantial weight loss of approximately 6% was observed at 200–800 °C. The NCQD surface functional groups were absorbed by the nanoparticles, resulting in a total weight loss of roughly 11% at approximately 800 °C. The DT analysis of the catalyst (Fig. 12b) generally shows two peaks: an endothermic peak around 120 °C is due to the release of absorbed water molecules, and an exothermic peak at 470 °C is due to the decomposition of organic molecules that were intact with the catalyst. This demonstrates the catalyst's resilience at high temperatures.

3.2.1 Catalytic performance of the Fe_3O_4CuO@CQD nanocomposite for reduction of 4-NA. To check the catalytic efficiency of the Fe_3O_4/CuO@CQD nanocomposite, the reduction of 4-nitroaniline was conducted, where Fe_3O_4/CuO@CQD nanocomposite was used as a catalyst and $NaBH_4$ was used as a reducing agent. The UV-visible spectrum analysis revealed that the 4-NA solution exhibited an absorption maximum of 380 nm. Upon the addition of $NaBH_4$ solution, the color of the solution transitioned to a bright yellow, and when 2 mg of the catalyst was added to the reaction mixture, peaks in the UV spectra started decreasing, which suggests the formation of *p*-phenylenediamine Fig. 13.

To further understand the role of various components, control tests were conducted under equal conditions. In the absence of $NaBH_4$, there was no discernible decrease of 4-nitroaniline, indicating that $NaBH_4$ is the necessary hydride source. Similarly, when $NaBH_4$ was present without the catalyst, very little reduction was seen, suggesting that electron transfer from BH_4^- to 4-nitroaniline is kinetically unfavourable in the absence of a catalyst. This indicates that, to achieve a swift

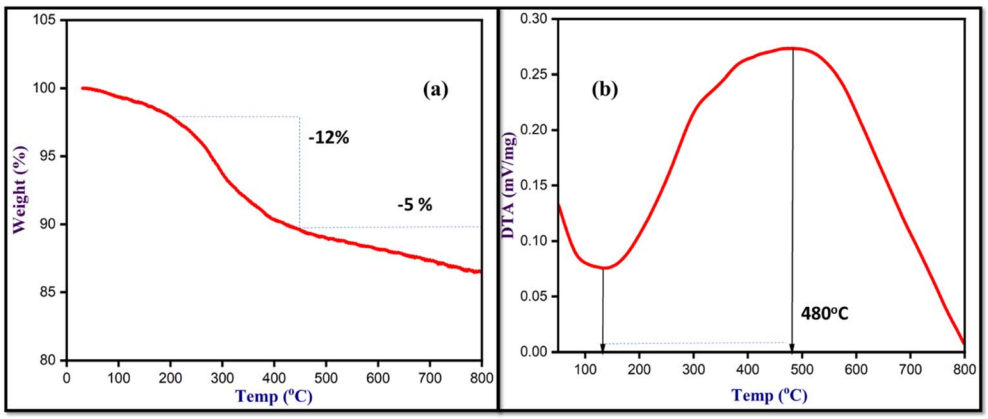

Fig. 12 (a) TGA and (b) DTA analyses of the Fe_3O_4/CuO@CQD nanocomposite.

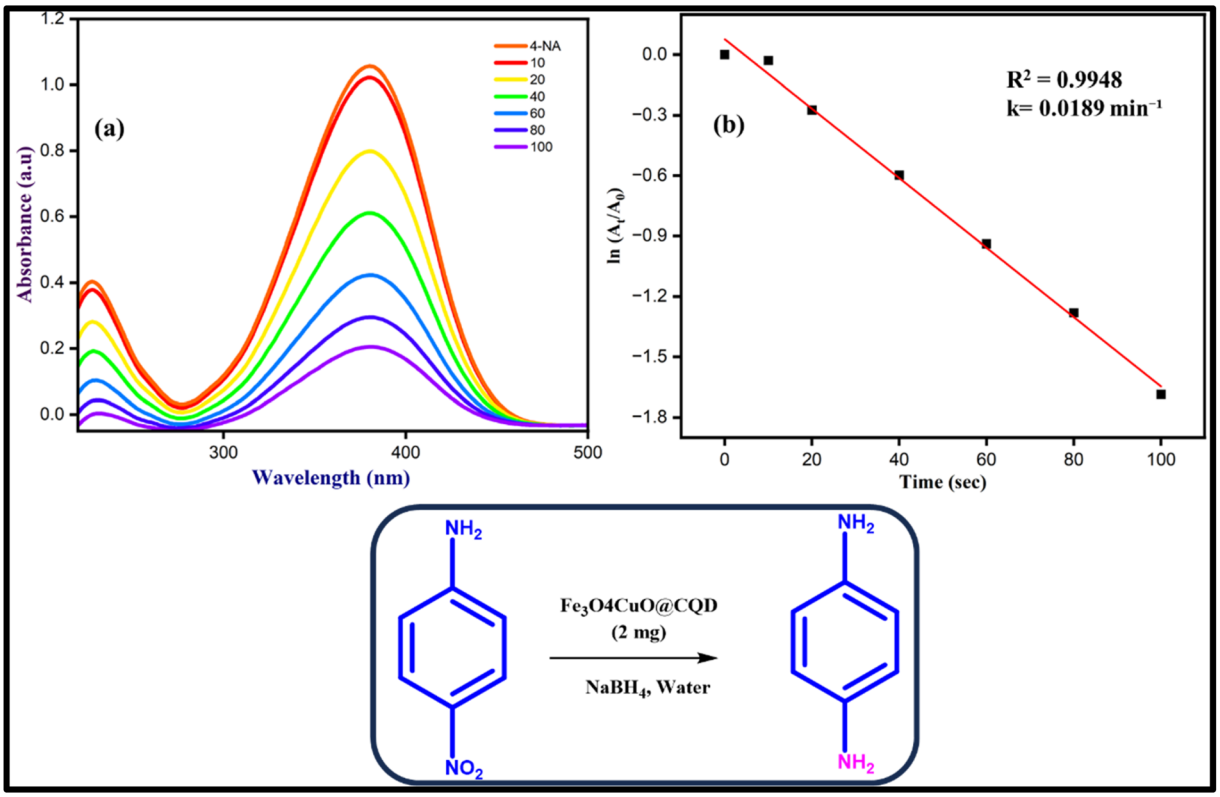

Fig. 13 Reduction of 4-nitroaniline (a) UV-visible analysis and (b) kinetic plot for the reduction of nitrophenol.

reduction of 4-NA, the experiment requires the presence of both catalysts and $NaBH_4$. When the experiment was conducted separately with Fe_3O_4 and CuO as different individual catalyst the reduction rate was quite slower as compared to the nanocomposite. When the active site of both the catalysts combines with the NCQDs, it inhibits nanoparticle aggregation and allow electron transport, which is responsible for the composite's increased activity.

The analysis of the chemical kinetic plot in Fig. 13 revealed a rate constant of $k = 0.0189\ min^{-1}$, accompanied by an R^2 value of 0.9948. The elevated concentration of $NaBH_4$ suggests that this reaction adheres to pseudo-first-order kinetics.

4 Conclusion

In this study, the NCQDs were successfully synthesized using raw turmeric and L-arginine *via* an eco-friendly hydrothermal method and demonstrated multifunctional applications. This NCQD was chosen as an excellent choice for the selective detection of 4-NP and radical scavenging activities for DPPH due to their unique photoluminescence and therapeutic behaviours. Additionally, Fe_3O_4CuO@CQD nanocomposite was synthesized using the NCQD, where it acted as a stabilizing agent. This Fe_3O_4CuO@CQD nanocomposite, which was highly efficient and magnetically recoverable, acted as a catalyst for the reduction of 4-nitroaniline. Altogether, this study showcases the compatibility of the NCQDs as a multifunctional gateway towards sensing, antioxidant activities, and stabilization of Fe_3O_4CuO@CQD nanocomposite.

Conflicts of interest

There are no conflicts to declare.

Data availability

The data supporting this article have been included as part of the supplementary information (SI). Supplementary information: additional supporting data and characterisation results. See DOI: https://doi.org/10.1039/d6ra00058d.

References

1 D. Elango, J. S. Packialakshmi, V. Manikandan and P. Jayanthi, *Mater. Lett.*, 2022, **312**, 131667.
2 S. H. Choi, *J. Phys. D: Appl. Phys.*, 2017, **50**, 103002.
3 P. N. Joshi, S. Kundu, S. K. Sanghi and D. Sarkar, *Smart Drug Delivery System*, 2016, vol. 7, pp. 159–195.
4 J. Dhariwal, G. K. Rao and D. Vaya, *RSC Sustainability*, 2024, **2**, 11–36.
5 S. Gulati, A. Baul, A. Amar, R. Wadhwa, S. Kumar and R. S. Varma, *Nanomaterials*, 2023, **13**, 554.
6 Y. J. Jiang, M. Lin, T. Yang, R. S. Li, C. Z. Huang, J. Wang and Y. F. Li, *J. Mater. Chem. B*, 2019, **7**, 2074–2080.
7 Y. Liu, X. Gong, W. Dong, R. Zhou, S. Shuang and C. Dong, *Talanta*, 2018, **183**, 61–69.
8 J. Liang, W. Li, J. Chen, X. Huang, Y. Liu, X. Zhang and H. Zhang, *ACS Appl. Bio Mater.*, 2021, **4**, 6937–6945.

9 X. Dong, W. Liang, M. J. Meziani, Y. P. Sun and L. Yang, *Theranostics*, 2020, **10**, 671–686.
10 A. Tadesse, N. Belachew, M. Hagos and K. Basavaiah, *J. Fluoresc.*, 2021, **31**, 763–774.
11 D. Dey, T. Bhattacharya, B. Majumdar, S. Mandani, B. Sharma and T. K. Sarma, *Dalton Trans.*, 2013, **42**, 13821–13825.
12 E. Seliverstova, N. Ibrayev and E. Menshova, *Fullerenes, Nanotubes Carbon Nanostruct.*, 2022, **30**, 119–125.
13 W. Li, Z. Zhang, B. Kong, S. Feng, J. Wang, L. Wang and D. Zhao, *Angew. Chem., Int. Ed.*, 2013, **52**, 8151–8155.
14 Q. Xu, T. Kuang, Y. Liu, L. Cai, X. Peng, T. S. Sreeprasad and N. Li, *J. Mater. Chem. B*, 2016, **4**, 7204–7219.
15 M. Nagaraj, S. Ramalingam, C. Murugan, S. Aldawood, J. O. Jin, I. Choi and M. Kim, *Environ. Res.*, 2022, **212**, 113273.
16 G. Ge, L. Li, M. Chen, X. Wu, Y. Yang, D. Wang and C. Guo, *Nanomaterials*, 2022, **12**, 986.
17 Y. Liu, Q. Zhou, J. Li, M. Lei and X. Yan, *Sens. Actuators, B*, 2016, **237**, 597–604.
18 P. Zhao, X. Li, G. Baryshnikov, B. Wu, H. Ågren, J. Zhang and L. Zhu, *Chem. Sci.*, 2018, **9**, 1323–1329.
19 C. Wang, M. Yang, H. Shi, Z. Yao, E. Liu, X. Hu and J. Fan, *Dyes Pigm.*, 2022, **204**, 110431.
20 M. Xu, S. Xu, Z. Yang, M. Shu, G. He, D. Huang and Y. Zhang, *Nanoscale*, 2015, **7**, 15915–15923.
21 M. D. El-Shazly, M. Opoku and G. W. Beall, *Sci. Rep.*, 2024, **14**, 16405.
22 F. Wen, P. Li, H. Yan and W. Su, *Carbohydr. Polym.*, 2023, **311**, 120784.
23 H. Tang, Y. Tang, H. Zhu, M. Xiao and M. Guo, *J. Mol. Struct.*, 2022, **1251**, 132034.
24 R. Umami, F. A. Permatasari, C. D. D. Sundari, F. Muttaqien and F. Iskandar, *J. Phys.: Conf. Ser.*, 2022, **2243**, 012043.
25 J. A. Jaleel and K. Pramod, *J. Controlled Release*, 2018, **269**, 302–321.
26 Y. Esmaeili, F. Toiserkani, Z. Qazanfarzadeh, M. Ghasemlou, M. Naebe, C. J. Barrow and S. Jafarzadeh, *Adv. Colloid Interface Sci.*, 2025, 103414.
27 X. W. Fang, H. Chang, T. Wu, C. H. Yeh, F. L. Hsiao, T. S. Ko and Y. W. Lin, *ACS Omega*, 2024, **9**, 23573–23583.
28 Z. U. Zango, K. H. Ibnaouf, A. Garba, O. Aldaghri, I. A. Wadi, A. Hosseini-Bandegharaei and O. Baigenzhenov, *J. Mol. Liq.*, 2025, 127497.
29 P. Singh, A. Mukherjee, A. Mahato, A. Pramanik and D. Dhak, *Chem. Afr.*, 2023, **6**, 561–578.
30 M. Sajjadi, N. Y. Baran, T. Baran, M. Nasrollahzadeh, M. R. Tahsili and M. Shokouhimehr, *Sep. Purif. Technol.*, 2020, **237**, 116383.
31 K. Shimada, K. Fujikawa, K. Yahara and T. Nakamura, *J. Agric. Food Chem.*, 1992, **40**, 945–948.
32 V. Mishra, A. Arya and T. S. Chundawat, *Curr. Organocatal.*, 2020, **7**, 23–33.